We are IntechOpen, the world's leading publisher of Open Access books Built by scientists, for scientists

6,900
Open access books available

185,000
International authors and editors

200M
Downloads

Our authors are among the

154
Countries delivered to

TOP 1%
most cited scientists

12.2%
Contributors from top 500 universities



WEB OF SCIENCE™

Selection of our books indexed in the Book Citation Index in Web of Science™ Core Collection (BKCI)

Interested in publishing with us?
Contact book.department@intechopen.com

Numbers displayed above are based on latest data collected.
For more information visit www.intechopen.com



11

An Efficient Adaptive Antenna-Impedance Tuning Unit Designed for Wireless Pacemaker Telemetry

Francis Chan Wai Po[1], Emeric de Foucauld[2], Jean-Baptiste David[2], Christophe Delavaud[2] and Pascal Ciais[2]
[1]*Institut Supérieur d'Electronique de Paris,*
[2]*CEA LETI MINATEC,*
France

1. Introduction

Since its first implantation into human body in 1958, pacemaker has known several evolutions [1-2] to become nowadays a vital cardiovascular device frequently prescribed to improve the quality of life for hearth failure patients. To increase the quality of service, pacemaker industry tends to integrate wireless telemetry technology into the medical device to allow home monitoring of the patient. Home monitoring technology challenges to analyse and to diagnose while the patient is sitting or sleeping at home.

The pacemaker radio communication module, designed to exchange data with an external base station, features new technologies including, but not limited, new architecture, low power design technique, acoustic wave filter co-integration, miniaturized antenna design, etc. The miniaturized antenna embedded on the pacemaker device is typically a narrow bandwidth high-Q antenna [3] easily detuned by unpredictable near field environmental factors [4-6]. The input impedance of the implanted antenna can vary due to the tissue (muscle, fat, skin, etc.) properties, thickness, and also the individual properties which differ from one person to another. In addition, the patient position and more generally the nearby objects may cause also change in the antenna input impedance. Mismatch of the antenna impedance significantly degrades the transmitter radiated output power, the receiver sensitivity, and therefore the power efficiency of the radio transceiver.

To highlight the possible random variability in the antenna input impedance that contributes to generate more or less important mismatch losses, precise characterization of the pacemaker antenna using different realistic human models is needed. In this way, electromagnetic simulations and measurements of the input impedance of the antenna immersed into homogeneous and heterogeneous human model were performed.

To guarantee the success of the wireless communication even in the presence of mismatch losses, traditional solution over specifies the design of the RF power modules consuming more energy at the expense of the battery lifetime. This solution is obviously not mandatory where a targeting lifetime at least greater than seven years is required for such implantable medical device. More suitable solution is focused on the addition of an adaptive antenna-impedance tuning unit to automatically match the antenna input impedance to the optimal impedance of the RF front-end radio communication module.

Most of existing antenna-impedance tuning units [7-15] operates iteratively to successfully adapt source and load impedances. However, iterative methods generally spend several hundred milliseconds to calibrate the system and are not well suited to low power pacemaker applications where energy is lost during the calibration as the proper state configuration of the system is not yet obtained.
The design of an energy efficient antenna-impedance tuning units based on a single step calibration method is proposed in this chapter to achieve a low power automatic matching process. The proposed method aims to extract the antenna complex impedance value in order to calculate the parameters of the network that match the extracted antenna impedance to the impedance of the RF power module at a selected frequency.
In this chapter, we describe briefly the pacemaker telemetry system, the design constraints and the limitations in section II. Since the pacemaker antenna is easily detuned by tissues, we challenge to characterize the impedance of the antenna immersed into different realistic human model in section III. In section IV, we propose a novel antenna impedance tuning method based on a single step process calibration to adapt automatically the antenna impedance to the optimal impedance of the front-end radio.

2. Pacemaker telemetry overview

Pacemaker industry is entering into the era of home monitoring technology. Home monitoring enables pacemaker's patients to be remotely followed-up via secured wireless or telephone networks as shown in Fig. 1. Depending on the patient's health status, the transfer of information could be done daily, weekly or monthly, and can be also triggered by the patient himself if he feels symptomatic. Home monitoring enhances patient safety and comfort, reduces pacing clinic visits and trips to the emergency room cutting down the overall healthcare costs and help the physicians better understand the patient's condition in less time.

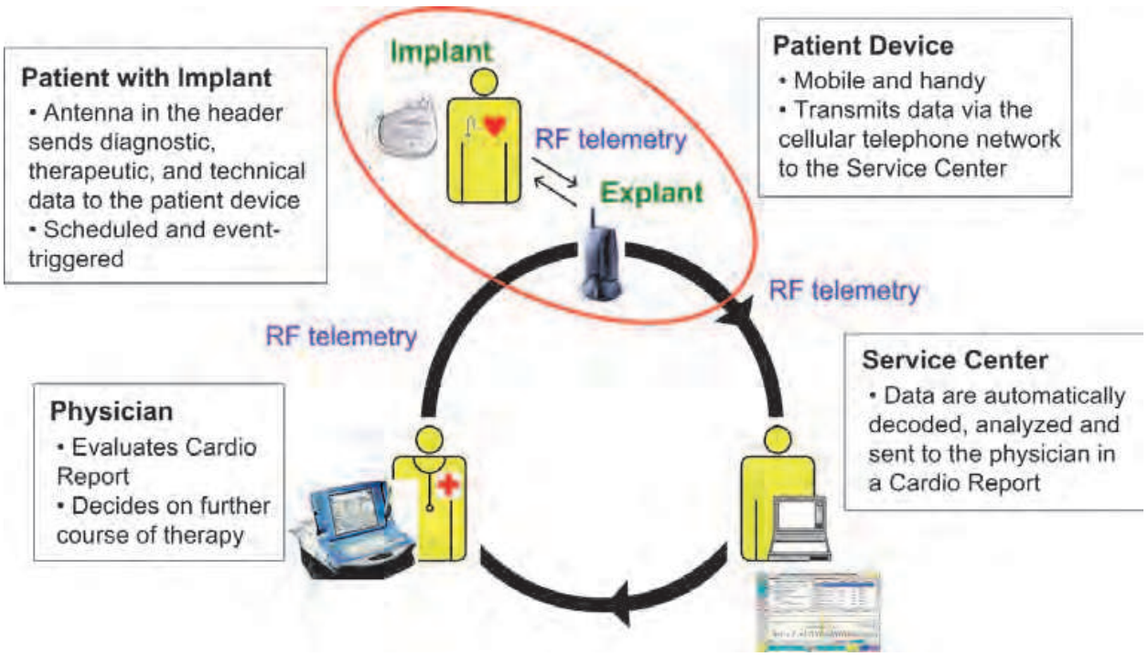


Fig. 1. Pacemaker home monitoring telemetry system

To allow home monitoring of the patient, it is necessary to integrate a wireless telemetry system into the medical device. Implantable pacemaker telemetry system provides a means for receiving downlink information from an external base station to the implanted medical device, and for transmitting uplink signals from the implanted device to the external unit.

2.1 Proposed wireless medical telemetry

Pacemaker microsystem typically embeds a controller, electrocardiogram (ECG) sensors and few analogue electronics blocs. In addition, the new generation device includes a wireless telemetry functionality which simplified bloc diagram is illustrated in Fig. 2. As the size of the final product should not be larger than its predecessor, it is necessary to tend towards a large scale integration of memory, controller, RF functionality including RF MEMS as well as analogue RF circuits.

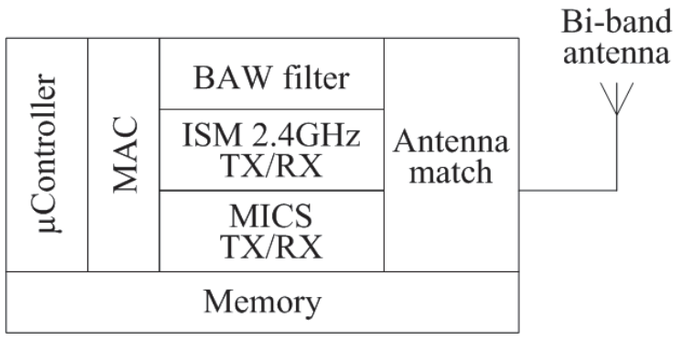


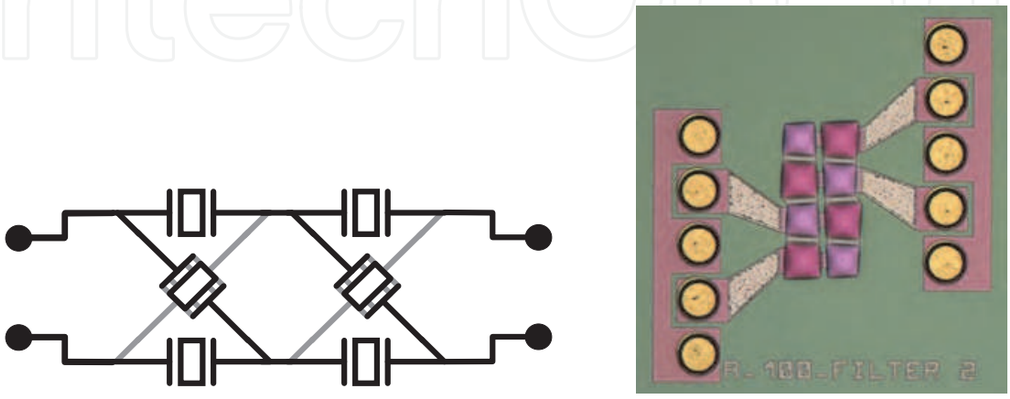
Fig. 2. Simplified bloc diagram of the pacemaker's wireless telemetry

The proposed wireless telemetry system integrates transceivers operating respectively at the Medical Implant Communication Service (MICS) frequency band and at the 2.4 GHz Industrial Medical Scientist (ISM) frequency band. The MICS 402-405 MHz frequency band is used to transmit short range secured data and for emergency link because only the exclusive MICS band is acknowledge as safe for medical devices by Food and Drug Administration (FDA). The ISM 2.4 GHz transceiver is dedicated for the implementation of a needed ultra low power wake up system and for transmitting data under higher equivalent isotropically radiated power (EIRP) to achieve the demanded increased communication range. In addition to the bi-band transceiver, a Bulk Acoustic Wave (BAW) filter and naturally a miniaturized loop antenna are embedded into the medical microsystem.

2.1.1 BAW Filter design and integration

The filter was implemented to address the high level risk of electromagnetic interferences in the widely used ISM 2.4 GHz frequency band using Solid Mounted Resonators (SMR). The resonators in SMR structures are realized on the top of an acoustic mirror structure based on the Bragg reflector principle [16]. The resonators layers were composed of classical couple AlN-Mo. In contrast to [17], the Bragg reflector was implemented using an exclusive dielectric stack composed of SiOC:H and SixNy. The acoustical performance of the fully dielectric stack is comparable to traditional SiO2-W reflectors. However, this fully dielectric configuration strongly reduces the electrical coupling between resonators, and ensures high

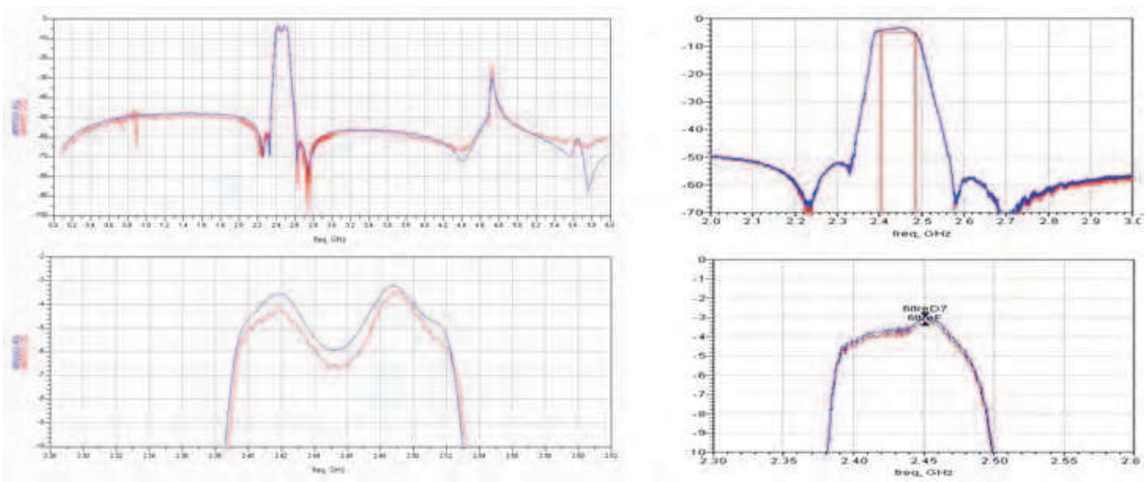
out-of-band rejection. Zero level packaging ensures a micro-cavity on the upper side of the resonator, thanks to a released bi-layer SiO2/BCB.
The filter is based on a double-lattice topology (Fig. 3 (a)) and series inductances of maximum 1nH can be added so as to increase slightly the bandwidth, or for matching considerations. The photography in Fig. 3 (b) shows the 2.4 GHz filter. The active area is 450x225µm², and the complete die is 1mm². 120µm diameter areas with a 150µm pitch were prepared for bumping as well as for probe testing.



(a) (b)

Fig. 3. Double lattice BAW filter (a) topology (b) photography

Flip-chip on CMOS and LTCC technologies were studied for the integration of the filter. As illustrated in Fig. 4 (a), flip chip on CMOS integration approach exhibits limited performances for several reasons. The CMOS technology is based on a lossy substrate which give low performances interconnects. As consequences, wide pad bumps are strongly capacitive and minimum distance between bumps and pad ring gives long and lossy lines.



(a) (b)

Fig. 4. BAW filter responses (a) Flip chip on CMOS measurement and simulation (b) Stand alone BAW filter versus flip chip on LTCC

In order to get better performance in the antenna to CMOS link, an alternative design has been also investigated to assemble the BAW filter with the antenna matching network in a same LTCC die, leading to a SiP approach. The comparison between on-probe BAW measurement and the flip-chipped BAW on LTCC is illustrated in Fig. 4 (b) where the responses are very close each other. Less than 0.2 dB additional insertion loss is observed.

2.1.2 Miniaturized antenna

A miniaturized loop antennas for implanted medical device designed to operate at both MICS 402-405 MHz and ISM 2.4 GHz frequency bandwidths have been successfully fabricated [18-21]. As illustrated in Fig. 5, the designed rectangular loop antenna embedded in a titanium (σ=2.3×10^6 S/m) housing biocompatible pacemaker prototype is made of copper (σ=5.8×107 S/m) covered with a silicone layer (ε_r=2.8) for biocompatibility. The physical dimensions of the rectangular loop antenna are approximately equal to 29.5 mm width and 18 mm height.

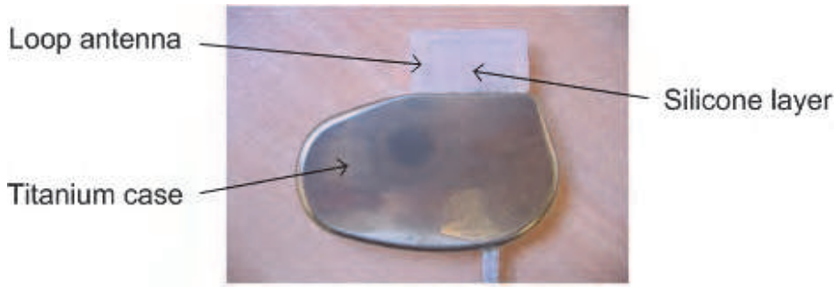


Fig. 5. Miniaturized loop antenna embedded in a pacemaker prototype

2.2 Transceiver design constraints and limitations

Medical devices require ultra low power, high performance transceiver. The design considerations of such transceivers are subjected to strong technical challenges which basic requirements [22] are as follows:

- Low power during communication is required since the battery power is limited. During communication sessions, current should be less than 6mA for most implantable device.
- Mostly in asleep mode, a designed ultra low power ISM 2.4 GHz receiver should periodically look for wakeup signal.
- As the size of the device should be continuously reduced, minimum external components is mandatory. High scale integration should also reduce significantly costs and increase the overall system reliability.
- Higher data rates, reliability are targeted.
- Good selectivity and interference rejection.
- Increase of the communication range greater than 2 meter range.

In such medical microsystem, over specify the system consumes more energy, reduces the battery lifetime and is therefore not mandatory to improve the limited communication range. Longer range implies the design of an automatic power optimized system. Thus, the integration of an automatic antenna tuning unit should contribute to improve the budget

link by reducing the power losses due to impedance mismatch of the body affected small antenna.

3. Antenna input impedance characterization

The miniaturized high-Q loop antenna impedance is highly dependant on the close environment of this antenna. Due to the unpredictable near field tissues properties, its thickness variation or patient's position change, the antenna impedance can vary introducing some quite variable losses due to mis-adaptation. To address this problem, it can be advantageous to design a tunable matching network to improve the adaptation where the variability range of the network should be able to match the variation range of the antenna impedance to the optimal impedance of the front-end radio. Therefore, there is a first need that consists in the characterization of the variability in the antenna input impedance in order to decide of the matching topology. In so far as the approach is the same whatever the chosen frequency, we decide to focus our work considering the MICS frequency band.

3.1 Human body modeling

Generally, antenna impedance is characterized in homogeneous lossy dispersive fluids which simulate the average human body electrical properties. As impedance characterization requires to know the electromagnetic field behaviour in near antenna area, only reduced volume of these lossy materials is modelled. But, to accurately take into account the near field pacemaker antenna behaviour, different human tissues close to the implant have to be also considered. This will be done by using heterogeneous model with limited dimensions as multi-layered structures or as existing accurate human model of electromagnetic simulation tool.

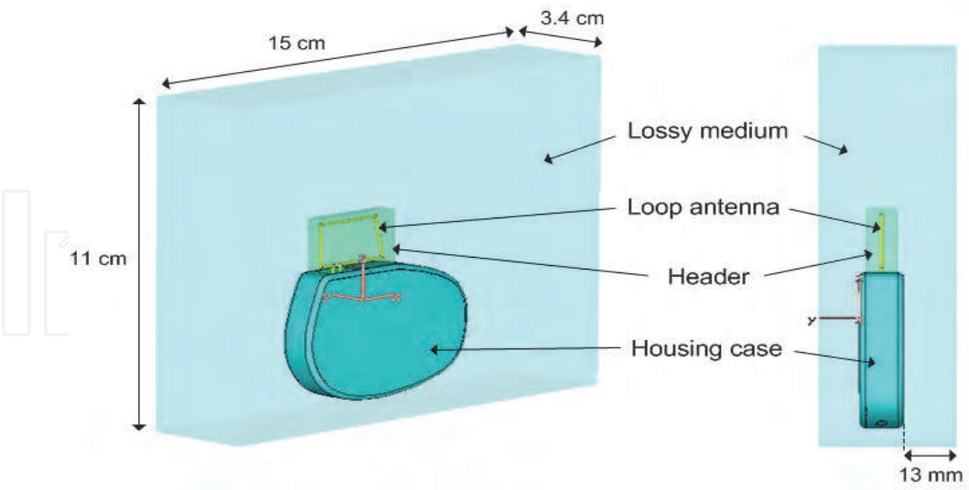
3.1.1 Homogeneous model

The pacemaker implant is plunged in a dispersive and lossy liquid material with frequency dependent electrical properties. In order to characterize antenna pacemaker impedance in the 402-405 MHz MICS frequency band, the 450 MHz body tissue equivalent liquid is used. The target electrical parameters of this fluid (conductivity σ and real part of permittivity ε_r') are provided by the FCC [23], as given in Table 1.

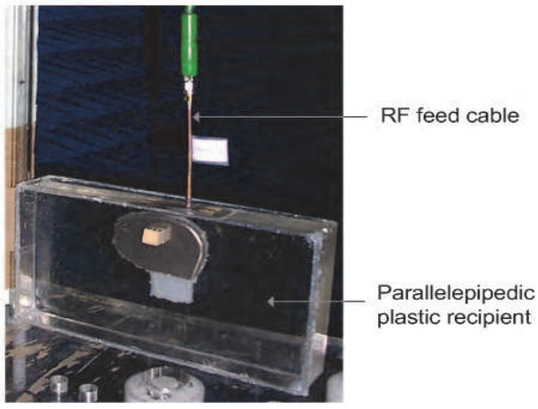
	Permittivity (ε_r')	Conductivity (σ, S/m)
Target values	56.7	0.94
Measured values	56.2	0.95

Table 1. Body simulating liquid electrical properties at 450 MHz

In the electromagnetic simulation tool based on Finite-Integration Time-Domain (FITD) method (CST Microwave Studio) [24], the homogeneous liquid model is represented by a parallelepiped (15cm×11cm×3.4cm). The rectangular homogeneous block dimensions and the pacemaker inside it as illustrated in Fig. 6 (a) are optimized for the heterogeneous model. For the experimental setup in Fig. 6 (b), the pacemaker is plunged into a rectangular plastic recipient filled with homogeneous liquid and which dimensions are the same than the simulated one.



(a)



(b)

Fig. 6. Homogeneous model (a) simulated configuration (b) experimental set-up

3.1.2 Heterogeneous model

The implantable device is inserted in three heterogeneous models: the heterogeneous human model named Hugo which is the simulation tool human model [24], a multi-layered structure and a simple experimental setup made to validate simulated heterogeneous models, the "human + hand" model. Compared to previous homogeneous model, the main advantage of these heterogeneous models is the ability to carefully model all human tissues in near antenna area to accurately take into account the near field pacemaker antenna behaviour.

The pacemaker device is implanted in the pectoral of Hugo, in a limited volume sample of 11.2 x 6.4 x 11.6 cm^3 (Fig. 7 (a)). The voxel size of the human body model is the minimal voxel size of the simulation tool, i.e. 1 mm^3. The whole body phantom contains 44 different tissues, whose real part of permittivity (ε_r') and conductivity (σ) are taken from [24] at 450 MHz. The chosen limited sample obviously includes fewer tissues than the complete body model.

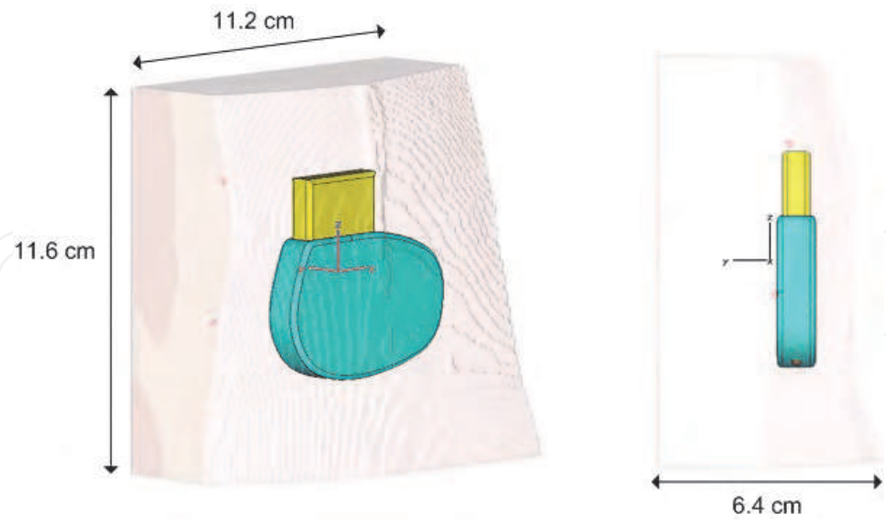


Fig. 7. Heterogeneous Hugo model

In order to easily design implanted antennas, multi-layered geometries which provide an acceptable model for the human body, were firstly proposed in [18]. Based on the real human body structure of the simulation tool, the heterogeneous multi-layered model used here (Fig. 8) is made of three layers (skin, fat, muscle) that have different thickness and different electrical properties. The thickness of the skin, fat and muscle tissues are respectively 4, 20 and 10 mm. The electrical properties of these three layers are taken from electrical data of human body phantom tissues and given in Table 2. The pacemaker is implanted in the fat layer just under the skin layer. The geometrical characteristics of the heterogeneous model, i.e. pacemaker position inside the rectangular block and dimensions of both layers and whole block, have been optimized in order to be in accordance with Hugo implant impedance.

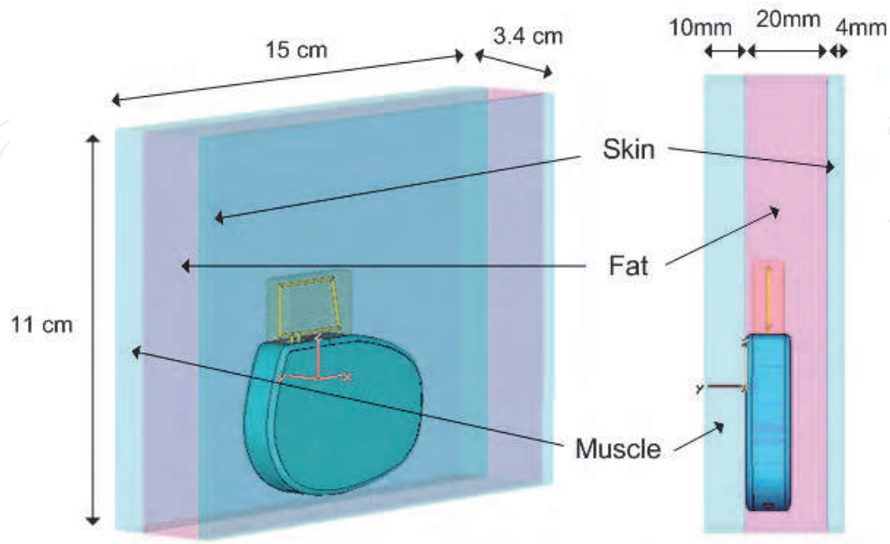


Fig. 8. Multi-layer heterogeneous model

Biological tissue	Permittivity (ε_r')	Conductivity (σ, S/m)
Fat tissue	5.560525	0.041934
Skin	45.753101	0.708836
Muscle	58.482101	0.851437

Table 2. Electrical data of human body phantom tissues

A simple experimental setup with a real human is also experimented. This one covers the pacemaker with his hand and puts it against his bust in exercising a strong pressure (Fig. 9). This setup has not the intention to replace an implantation in a realistic human body, but we will see in the next section that it constitutes a good approximation.



Fig. 9. "Human + hand" model

3.2 Results

The antenna input impedances characterized in homogeneous and heterogeneous models are respectively shown in Fig. 10 and Fig. 11. In homogeneous models, measured results with coaxial cable are systematically compared to simulated results with and without cable. In the configuration without cable, the loop antenna is fed by a lumped port which consists typically in a voltage applied between the two extremities of the loop. This configuration was used in order to simplify the numerical problem size to solve and thereby to reduce the total simulation time. Finally, only this simplified excitation setup will be used in accurate and heavy heterogeneous models because it allows fast simulation results to be obtained.

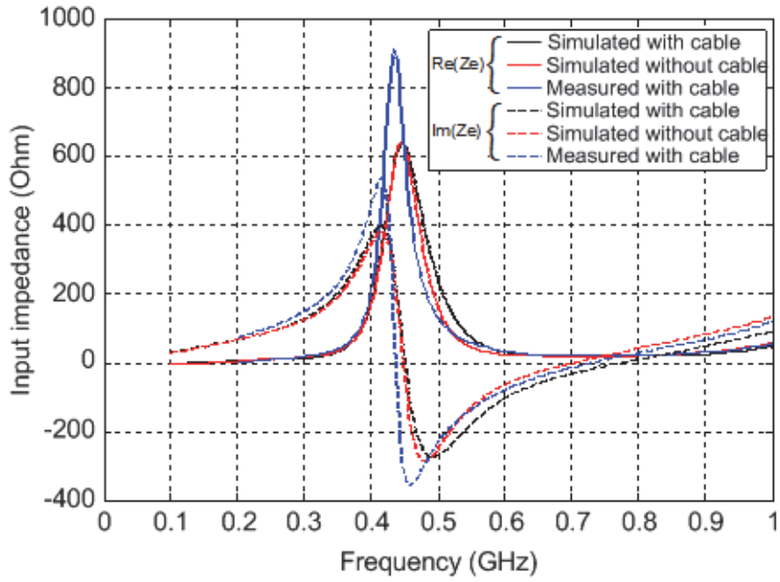


Fig. 10. Antenna impedance in homogeneous human models

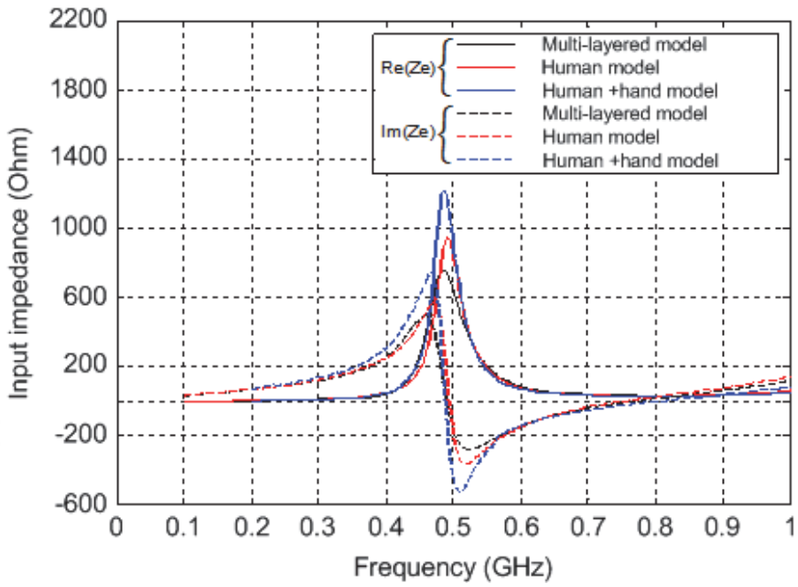


Fig. 11. Antenna impedance in heterogeneous human models

A global study of the impedance characteristics shows that the sensitivity of the antenna to the human tissues results in a shift of the resonant mode. As the MICS band is in the vicinity of this resonant frequency characterized by fast impedance variation, the shift of 50 MHz in frequency involves a huge shift in impedance levels (see Fig. 10 and Fig. 11); hence, while the values of real part of impedance in heterogeneous models are between 39 and 51 Ω, those in the homogeneous models are between 185 and 260 Ω. Similar discrepancies can be seen on imaginary part of impedance. These impedance random shifts are too significant to

be neglected. To allow maximum power transfer between transceiver circuitry and antenna, it is necessary to design a variable matching network able to match automatically the wide range of antenna impedance to the front-end radio.

4. Single step antenna tuning unit

To address the problem due to impedance mismatch, many antenna impedance tuning units operating iteratively and/or using directional coupler to evaluate the quality of the link were investigated [7-15]. Since the use of a bulky additional coupler into the device is totally inacceptable and since iterative matching process spends time and consumes power to set the proper state of the network, we investigate on a novel coupler less method [25] solving the problems related to the impedance mismatch in a single iteration. The proposed solution detailed in this section is the first system able to match automatically in a single process both TX and RX matching networks. It reduces the power losses in transmission and in reception contributing to the optimization of the power efficiency of the transceiver itself.

4.1 Brief description

In general, the power consumption of radio communication modules is dominated by the power consumption of the power amplifier during the transmitting path and by the power consumption of the low noise amplifier during the receiving path. Since antenna impedance calibration procedure is done during the transmitting mode, in order to achieve low power antenna impedance tuning unit, it is necessary to reduce strongly the time required for the calibration.

Therefore, we propose an innovative single step antenna tuning unit concept which basic topology is illustrated in Fig. 12. A generic detector made of capacitor C_{det}, which advantageously replaces the usual bulky coupler, is inserted between the power module and the tunable matching network. The sensed signal v_1 and v_2 are attenuated for linearity issue, down converted to a lower intermediate frequency and analyzed by a processor. As described by the flow chart in Fig. 13, the processor exploits the magnitude and the phase of the sensed signals v_1 and v_2 to first calculate the impedance Z_1 and/or Z_2 located in the left and the right port of the detector, respectively. Finally, the extraction of the antenna input impedance exploits the well known deembedding techniques to calculate Z_{Ant} from Z_1 or Z_2. The obtained antenna input impedance value is used to directly calculate the parameters of the matching network that reach the proper state of the system at a selected frequency.

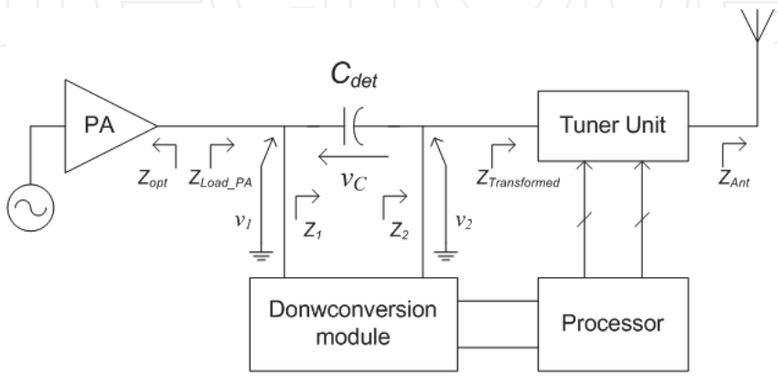


Fig. 12. Description of the proposed antenna tuning unit

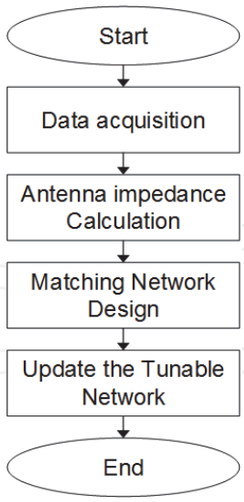


Fig. 13. Flow chart of the antenna tuning unit process

The success of the calibration with arbitrary source and load impedances is achieved with a single iteration. Since iteration is avoided, the matching time is strongly reduced by more than several hundred times compared to iterative optimization method to achieve high speed and low power consumption solution.

4.2 Proposed architecture and analysis

Here, we integrate the antenna tuning unit topology presented in Fig. 12 into the architecture of the MICS frequency band transceiver as illustrated in Fig. 14.

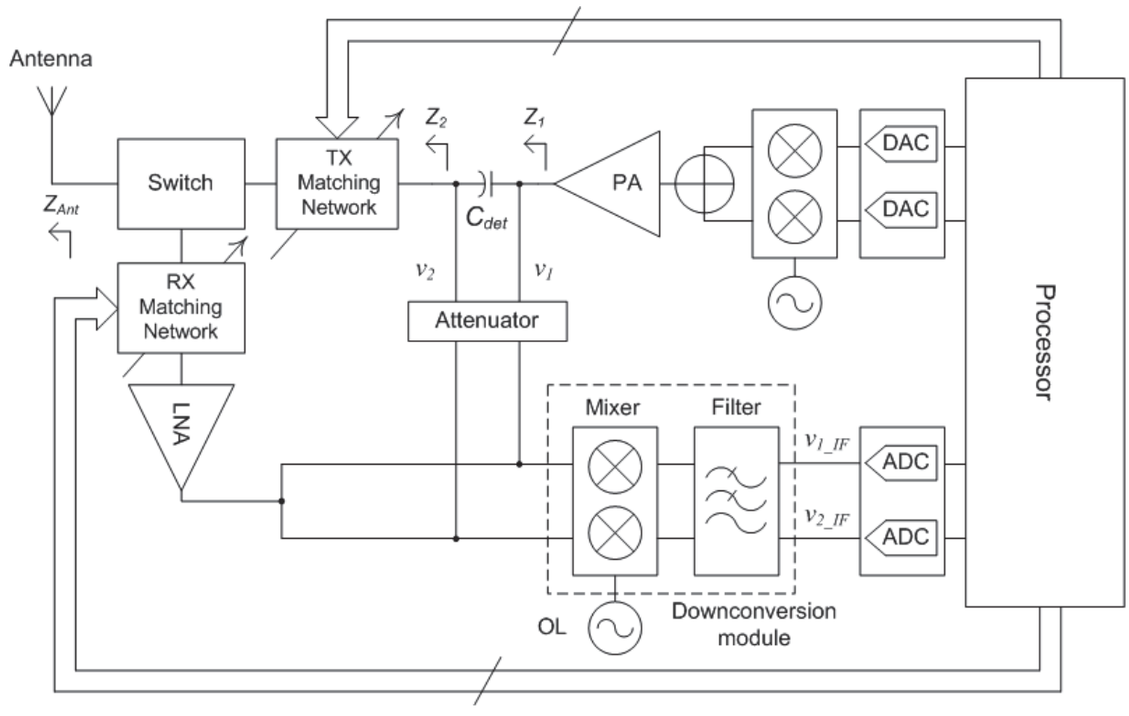


Fig. 14. Integration of the ATU into the architecture of the proposed MICS transceiver

The benefit of the proposed architecture is that the down conversion module and the baseband processor used for the design of the antenna tuning unit, as illustrated in Fig. 12 are already included into the MICS band transceiver [22]. Only minor extra hardware is therefore added for its implementation: a sensing module, an attenuator and tunable matching networks.
In addition to the TX tunable matching network, we insert a RX tunable matching network between the antenna and the front-end receiver in order to maximize the sensitivity of the receiver regardless of the value of the antenna impedance. Since the matching algorithm is able to match the extracted antenna impedance to the optimal impedance of the power amplifier, it is obviously possible to use the same program to match the antenna impedance to the input impedance of the low noise amplifier (LNA) optimizing the sensitivity of the receiver. This is to our knowledge the first antenna impedance tuning unit able to calibrate both the transmitter and the receiver in a same impedance matching process.

4.2.1 Sensing module

The sensing module made of a transmit capacitor C_{det} is inserted between the power amplifier and the TX tunable matching network. A capacitor is easy to integrate and its high quality factor advantageously limits the loss generated due to the sensing operation. However, the value of the capacitor C_{det} needs to be chosen carefully. To set the value of C_{det}, we analyze the impact of C_{det} on the degradation of the network transformation ratio and on the sensitivity of the detection.
As demonstrated in [26], the associated transformation quality factor Q of a network that matches a load resistance R_L to a source resistance R_S is

$$Q = \sqrt{\frac{R_S}{R_L} - 1} \qquad \text{if } R_S \geq R_L \tag{1}$$

$$Q = \sqrt{\frac{R_L}{R_S} - 1} \qquad \text{if } R_S \leq R_L \tag{2}$$

In the presence of the capacitor C_{det}, the expression of the equivalent source resistance is obtained exploiting the network series parallel transformation in Fig. 15.

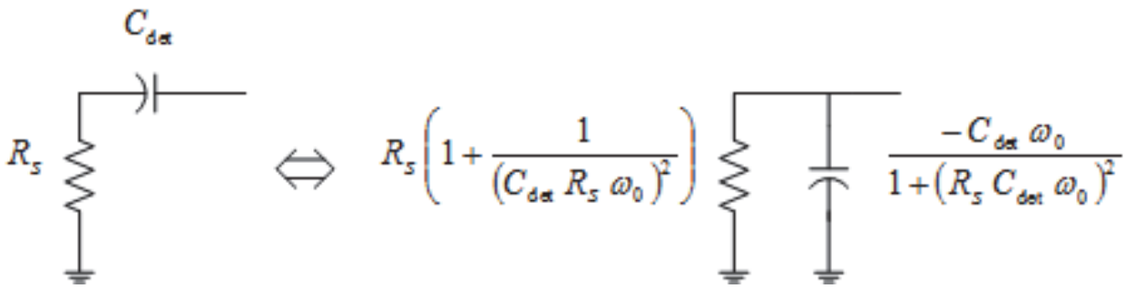


Fig. 15. Source equivalent resistance in the presence of C_{det}

The associated transformation quality factor Q of the network topology in the presence of C_{det} becomes

$$Q = \sqrt{\frac{R_S\left(1+\frac{1}{\left(C_{\det} R_S \omega_0\right)^2}\right)}{R_L} - 1} \qquad \text{if } R_S\left(1+\frac{1}{\left(C_{\det} R_S \omega_0\right)^2}\right) \geq R_L \tag{3}$$

$$Q = \sqrt{\frac{R_L}{R_S\left(1+\frac{1}{\left(C_{\det} R_S \omega_0\right)^2}\right)} - 1} \qquad \text{if } R_S\left(1+\frac{1}{\left(C_{\det} R_S \omega_0\right)^2}\right) \leq R_L \tag{4}$$

As demonstrated in [26], an increase of the transformation quality factor Q in (3) reduces the efficiency of a lossy matching network, whereas a decrease of Q in (4) offers a better efficiency. In order to limit the impact of C_{det} on the raise of Q in (3) and therefore on the degradation of the matching network efficiency, it is mandatory to set the C_{det} value greater than $1/(R_S \omega_0)$.

Moreover, as shown in Fig. 16, the sensing sensitivity depends on the value of C_{det}. In Fig. 16 (a), the range variation of the ratio v_2/v_1 is limited and centered around 1 and 0 for a strong and small value of C_{det}, respectively. An example of wide range variation of the ratio v_2/v_1 that provides a good sensitivity of the impedance sensing operation is illustrated in Fig. 16 (b) where C_{det} is equal to $1/(R_S \omega_0)$.

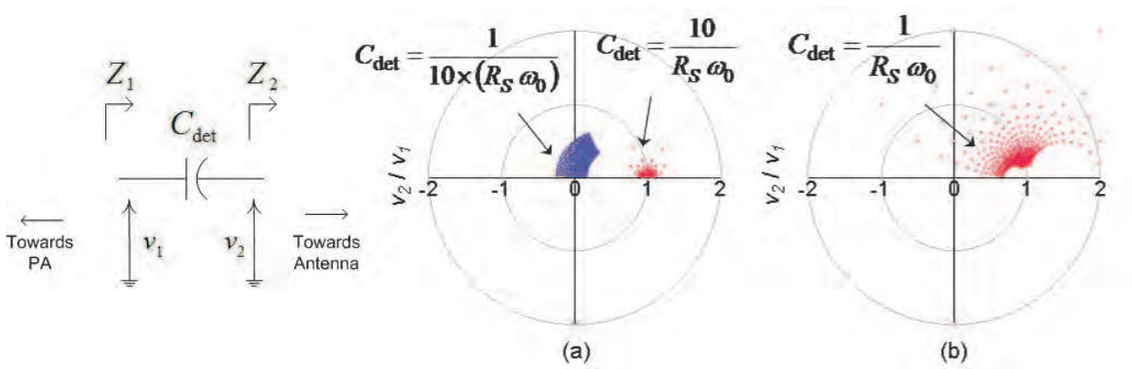


Fig. 16. Range variation of v2/v1 function of C_{det} value plotted in polar domain for $Re(Z_2) \in [10, 300]$ and $Im(Z_2) \in [-100, 100]$

A tradeoff between the sensitivity of the impedance sensing and the degradation of the association transformation quality factor, that could reduce lossy matching network efficiency, gives the expression of C_{det} as follow

$$C_{\det} = \frac{2}{R_S \omega_0} \tag{3}$$

In this condition, neglecting the loss in capacitors and for R_S=100Ω , R_L=50Ω and Q_L=50, a well matched single stage matching network will achieve a power efficiency [27] ($\eta \approx 1 - Q/Q_L$) of 98% and 97.55% without and with C_{det}, respectively. As the same, for R_S=50Ω, R_L=100Ω and Q_L=50, the power efficiency is this time improved from 98% to 98.45%.

4.2.2 Attenuator

An attenuator is inserted between the detection capacitor C_{det} and the down conversion module for linearity issue. Indeed, the magnitude of the signals v_1 and v_2 at the output of the power amplifier stage is large, whereas the input linearity of down conversion module made of mixer and channel filter is in general small. To avoid corruption of the wanted signals from undesirable harmonics generation, magnitude and phase errors due to AM/AM and AM/PM conversions in such nonlinear system, the attenuation value must be set so as to adapt v_1 and v_2 to the dynamic range of the down conversion module as shown in Fig. 17.

The 1-dB compression dynamic range $DR_{1\text{-dB}}$ of the down conversion module is the difference between the input 1-dB compression point *ICP1* and the sensitivity S_{min} of the donw conversion module. A back off is added to preserve the magnitude and phase integrity of the signals from AM/AM and AM/PM distortions. We obtain the dynamic range of the system as

$$DR = ICP1 - S_{\min} - Back\,off \tag{5}$$

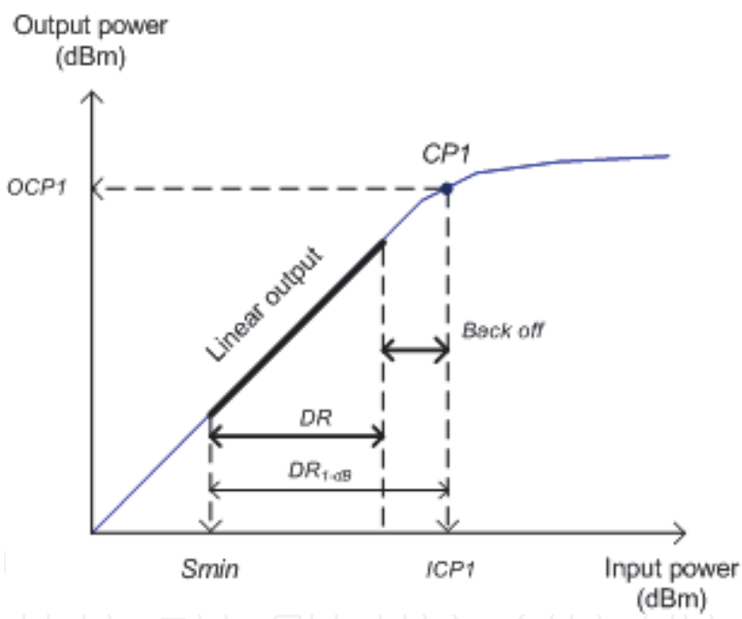


Fig. 17. Dynamic range of the down conversion module

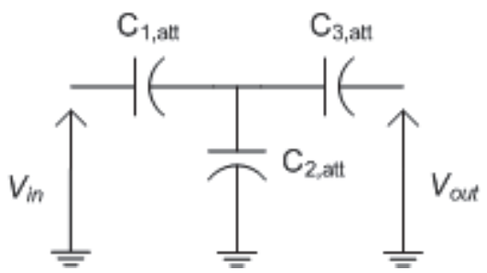


Fig. 18. Proposed capacitive attenuator

We basically implement a capacitive voltage divider as represented in Fig. 18 dedicated to the attenuation of v_1 and v_2. The value of the input capacitance $C_{1,att}$ is small enough to achieve good isolation, whereas the value of the shunted capacitor $C_{2,att}$ is strong and chosen to set the desired attenuation. $C_{3,att}$ is also small value capacitor and added to limit the impact the output load impedance on the attenuation.

4.2.3 Tunable matching network

The tunable matching network is needed for its ability to adapt a great number of load impedances or any change of load impedance to the source impedance. Single stage matching network ability to cover a wide range of impedance is relatively limited [28]. We prefer a generic low pass π matching network with complex load and source impedances as shown in Fig. 19. It is made of one fixed inductor and two variable capacitors made of diode varactors or bank of switched capacitors.

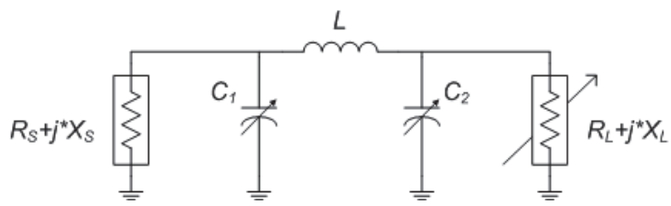


Fig. 19. Matching network with complex source and load impedances

As illustrated in Fig. 20, the ability of the network to match a load impedance range to the source impedance is strongly dependent on the inductance L value. Indeed, any normalized complex conjugate load impedance located in the dotted area can be matched to the source whereas any normalized impedance located in the forbidden region can not be adapted. As an example, let consider the poorly designed inductance L scenario in Fig. 20 (a). A part of the load impedance range, represented by the semicircular shape, is located in the forbidden region. To achieve the well-designed topology in Fig. 20 (b), the value of L must be set carefully.

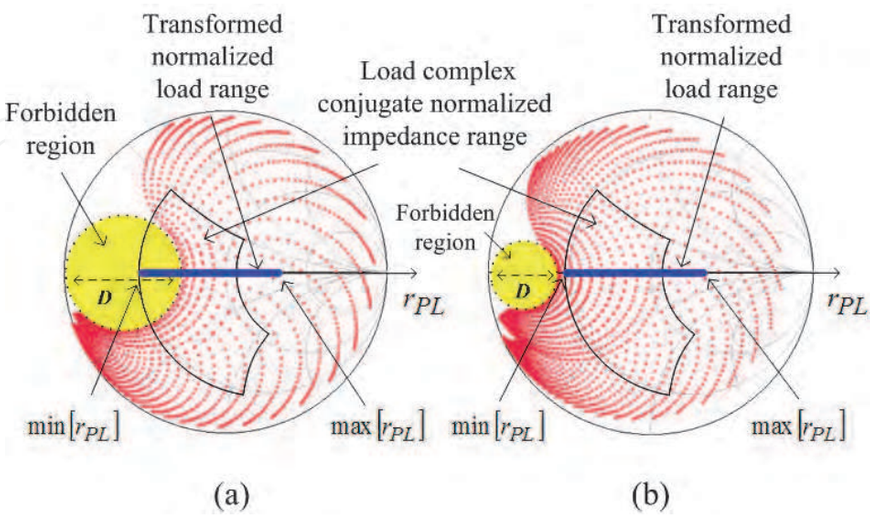


Fig. 20. Example of dynamic range of the impedance tuner (a) poorly inductance L designed scenario (b) well inductance L designed scenario

To facilitate the design of the inductance L value, we study the network in a real source and load impedance domain instead of complex source and load topology. A network transformation is computed and we obtain the matching network in Fig. 21 with real source and load impedances.

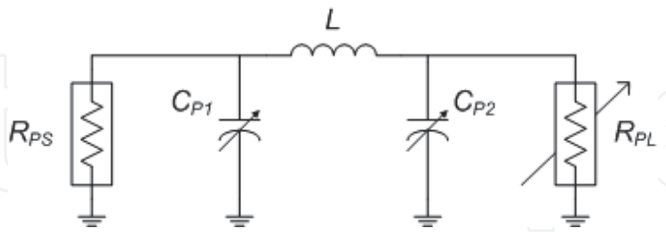


Fig. 21. Transformed matching network with real source and load impedances

The expression of the real source R_{PS} and real load R_{PL} are given by (6) and (7), respectively. The normalized real load impedance range varies from min(r_{PL}) and max(r_{PL}) as reported on the Smith charts in Fig. 20 by the blue bold lines.

$$R_{PS} = R_S\left(1 + Q_S^2\right) \quad \text{where } Q_S = -X_S/R_S \tag{6}$$

$$R_{PL} = R_L\left(1 + Q_L^2\right) \quad \text{where } Q_L = -X_L/R_L \tag{7}$$

As demonstrated in [27], at a given angular frequency ω, and neglecting the self resonant frequency of the elements, the forbidden circle where load impedance can not be matched to the source impedance has a diameter D function of the inductance L and given by

$$D = \left(\frac{L\omega}{R_{PS}}\right)^2 \tag{8}$$

Since r_{PL} should be outside the forbidden circle, the forbidden circle diameter should be smaller than

$$D_{\max} = \min\left(r_{PL}\right) = \frac{\min\left(R_{PL}\right)}{R_{PS}} \tag{9}$$

As a consequence, the value of the inductance L should be smaller than the inductance maximum value L_{max} which expression is

$$L_{\max} = \frac{R_{PS}}{\omega}\sqrt{\frac{\min\left(R_{PL}\right)}{R_{PS}}} \tag{10}$$

4.3 Matching processor algorithm

The architecture of the processor is illustrated in Fig. 22. It analyses the magnitude/phase information of the down converted signals v_{1_IF}, v_{2_IF} to extract the antenna input impedance Z_{Ant} used to calculate the proper state of the system. We detail in this section the steps of the algorithm that contribute to reach the goals. The impedances Z_1 and/or Z_2 are first

calculated and de-embedded to extract the antenna input impedance Z_{Ant}. A novel matching network design algorithm presented in [27] is finally run to adapt the antenna input impedance to the front-end power module (power amplifier and low noise amplifier).

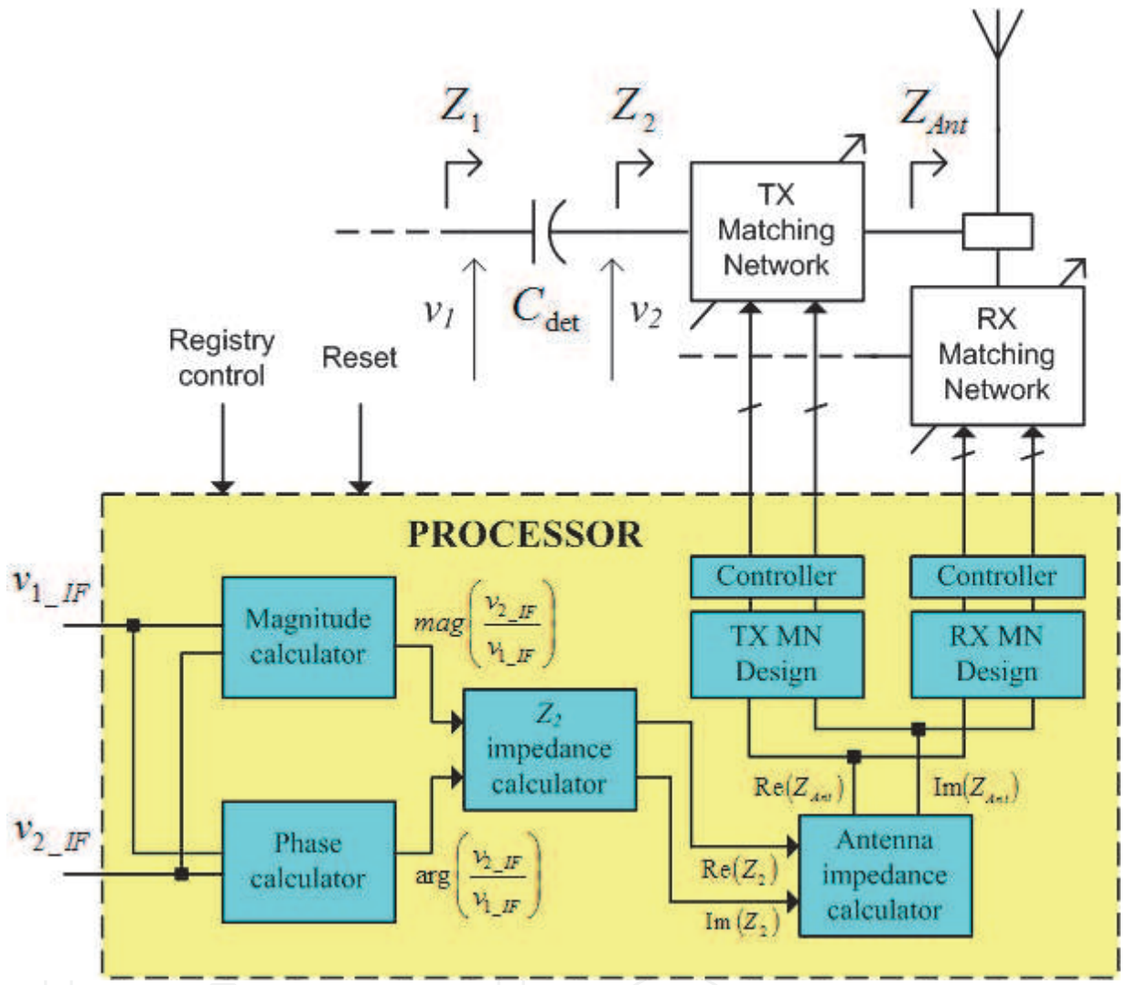


Fig. 22. Architecture of the ATU processor

4.3.1 Impedance calculation

Let consider the expression of $v_1(t)$ and $v_2(t)$ on the left and right terminals of C_{det} as

$$v_1(t) = A_1 \cos(\omega_0 t) \tag{11}$$

$$v_2(t) = A_2 \cos(\omega_0 t + \alpha) \tag{12}$$

where ω_0 is the angular carrier frequency, A_1 and A_2 are the magnitude of v_1 and v_2 respectively and α the phase shift.

The expression of the down converted signals $v_{1_IF}(t)$ and $v_{2_IF}(t)$ are

$$v_{1_IF}(t) = B_1 \cos(\omega_{IF} t) \quad \text{with} \quad B_1 = K \times A_1 \tag{13}$$

$$v_{2_IF}(t) = B_2 \cos(\omega_{IF}\, t - \alpha) \quad \text{with} \quad B_2 = K \times A_2 \tag{14}$$

From (11) (12) (13) and (14), we obtain the analytical expression for the voltage v_C across the detection capacitor C_{det} in the time domain as

$$v_{C\,\det}(t) = v_1(t) - v_2(t) = R\, \cos(\omega_0\, t - \sigma), \tag{15}$$

where,

$$R = \frac{1}{K}\sqrt{\left(B_1 - B_2\cos(\alpha)\right)^2 + \left(B_2 \sin(\alpha)\right)^2} \tag{16}$$

and,

$$\sigma = \arctan\left(\frac{B_2 \sin(\alpha)}{B_1 - B_2\cos(\alpha)}\right). \tag{17}$$

The impedance Z_1 at the left port of the detector C_{det} is

$$Z_1 = |Z_1| \times e^{j\times(\arg(Z_1))}, \tag{18}$$

where,

$$|Z_1| = \left|\frac{1}{jC_{\det}\omega_0}\right| \times \left|\frac{v_1}{v_{C\,\det}}\right| = \frac{B_1}{C_{\det}\,\omega_0\sqrt{\left(B_1 - B_2\cos(\alpha)\right)^2 + \left(B_2\sin(\alpha)\right)^2}}, \tag{19}$$

and,

$$\arg(Z_1) = \sigma - \frac{\pi}{2}. \tag{20}$$

Similarly, we obtain the impedance Z_2 at the right port of the detection capacitor C_{det} as

$$Z_2 = |Z_2| \times e^{j\times(\arg(Z_2))}, \tag{21}$$

where,

$$|Z_2| = \frac{B_2}{C_{\det}\,\omega_0\sqrt{\left(B_1 - B_2\cos(\alpha)\right)^2 + \left(B_2\sin(\alpha)\right)^2}}, \tag{22}$$

and,

$$\arg(Z_2) = \alpha + \sigma - \frac{\pi}{2}. \tag{23}$$

It is interesting to note that the impedances Z_1 and Z_2 at the ports of the detector are extracted with simplicity only from the magnitude B_1, B_2 and phase shift α of (v_{1_IF}, v_{2_IF}). The extraction of the antenna input impedance exploits the de-embedding techniques to

calculate Z_{Ant} from Z_1 or Z_2. For better results, input parasitic capacitance from the attenuator could be taken into account during the process.

4.3.2 Matching network design

The matching design algorithm exploits a novel method for synthesizing an automatic matching network summarized in Fig. 23 and previously presented in [27] in order to match the antenna input impedance Z_{Ant} to the optimal impedance of the power amplifier Z_{opt} and to the input impedance of the low noise amplifier. This method transforms the load and source complex impedances to real source and load impedances for simplicity. The parameters of the networks that achieve the proper state of the system are calculated exploiting the Smith chart in a novel way achieving the process with simple analytical expressions. By reducing the complexity of the algorithm, we reduce the number of instructions, the time required to calculate the optimal configuration of the tunable matching networks and the power consumption of the antenna impedance calibration unit.

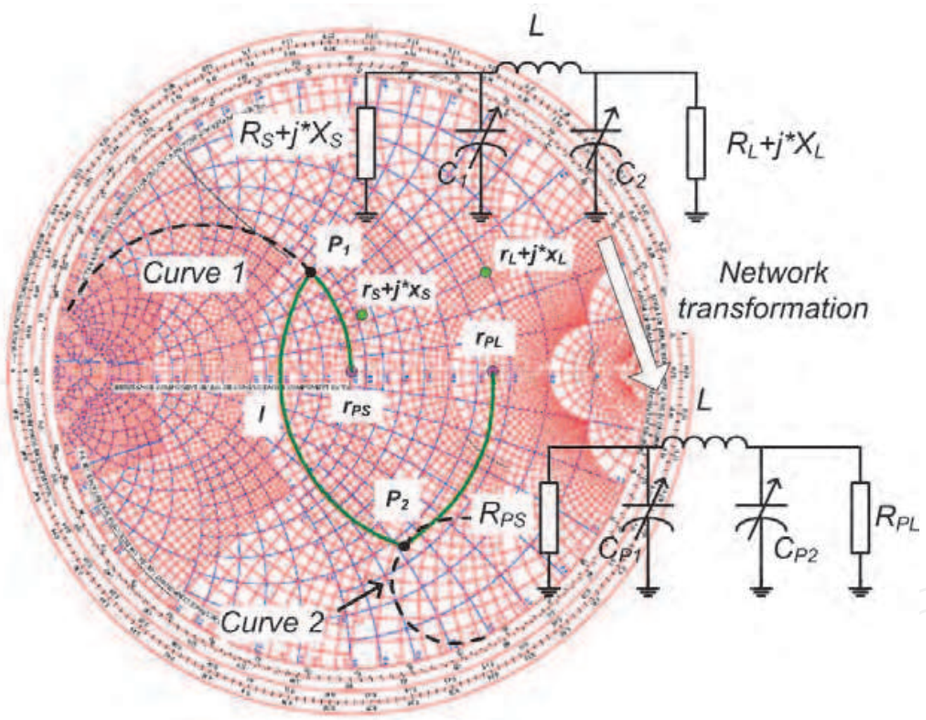


Fig. 23. Matching network design methodology presented in [27]

4.4 Results

A first experimental set-up of the antenna impedance tuning unit operating at the MICS 402-405 MHz frequency band was fabricated [29] as illustrated in Fig. 24. It includes the MICS frequency band demonstrator with only the TX low pass π tunable matching network, a microcontroller board and a pacemaker antenna immersed into a homogeneous human model liquid described in section III whose permittivity ε_r and conductivity σ are 56.2 and 0.95 S/m, respectively.

The demonstrator was made using a Flame Retardant 4 substrate (FR4) with a relative permittivity of 4.6, a dielectric loss tangent of 0.02 and a layer's thickness of 360 µm. The tunability of the low pass π matching network is realized by varactors which control voltages are decided by the microcontroller ADUC7026 from Analog Device. It is an ARM7TDMI based controller with a CPU that clocks up at 40MIPS. The signal carrier frequency is 403 MHz down converted to 256 kHz intermediate frequency and analyzed by the microcontroller for impedance matching consideration.

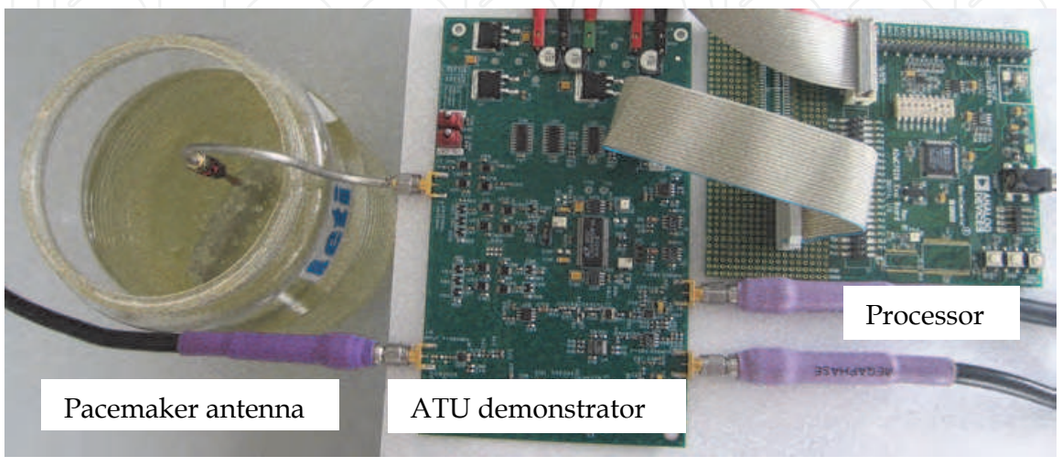


Fig. 24. ATU prototype including the pacemaker antenna

Fig. 25 shows two experimental reflection coefficient measurements. The first one plotted in Fig. 25 (a) was done before the calibration process in the presence of a detuned tunable low-pass π matching network. The second one illustrated in Fig. 25 (b) highlights a post-calibration reflection coefficient result up to -30 dB at the desired frequency of 403 MHz. As represented in Fig. 26, the proposed antenna tuning unit demonstrator spends no more than 900µs to realise the overall calibration process, including the data acquisition, the impedance calculation and the excecution of the matching network design algorithm.

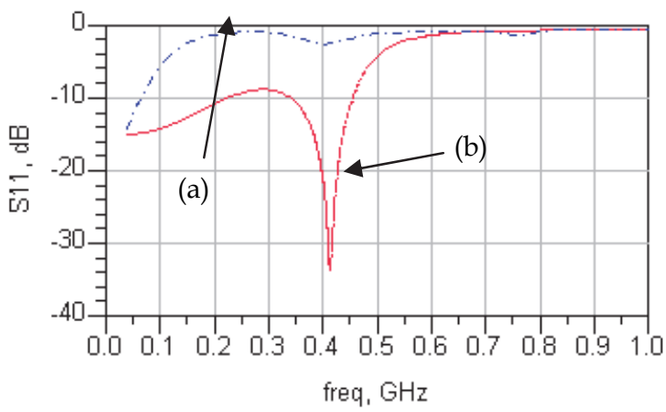


Fig. 25. Measured reflection coefficient (a) before the calibration process (a) after the proposed single step calibration

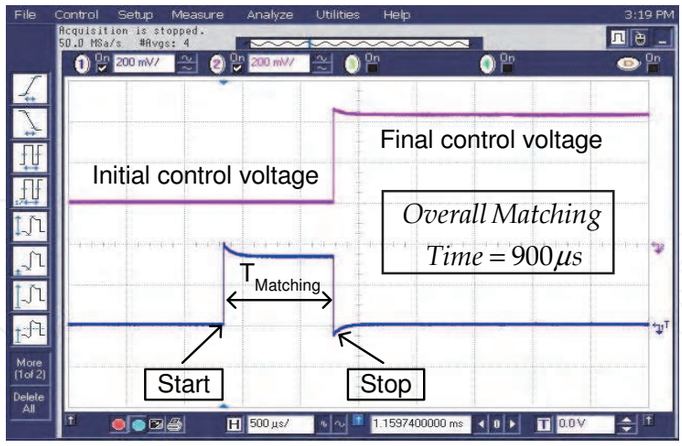


Fig. 26. Time Antenna calibration

5. Conclusion

New pacemaker tends to integrate a wireless telemetry system to allow home monitoring of the patient. The quality of service is strongly improved with an increase of safety, comfort and a reduction of cost. However, this challenge faces to a number of limitations like the need of low power high efficiency design, the degradation of the budget link while the antenna is immersed into the human body, etc. Indeed, it is demonstrated that the antenna impedance changes while immersed into human body causing mismatch of the antenna. To avoid antenna mismatch and reduction of the power efficiency of the radio link, we have proposed a new method to automatically match the antenna impedance to the front-end radio. This method operates in a single step to extract the antenna input impedance value exploited by a processor to match the antenna to the front-end radio both in transmission and reception. A demonstrator operating at the MICS 402-405 MHz frequency band was fabricated and an experimental set-up was presented. This prototype calibrates the system in less than 900µs with a 40MIPS clock processor to achieve a coefficient reflection S11 up to -30dB.

6. Acknowledgement

The authors would like to thank ELA Medical (SORIN Group) for supporting this work.

7. References

[1] Haddad, S.A.P., Houben, R.P.M., Serdijin, W.A (2006). The evolution of pacemakers, *IEEE Engineering in Medecine and Biology Magazine*, Vol. 25, Issue 3, pp. 38-48, Mars 2006

[2] Banbury, C.M. (1997). Surviving Technological Innovation in Pacemaker Industry 1959-1990, Garland Publishing Inc, ISBN 0815327967

[3] Wheeler, H.A. (1975). Small Antennas, *IEEE Transactions on Microwave Theroy and Techniques,* Vol. AP-23, No. 4, pp. 462-469, July 1975

[4] Boyle; K. (2003). The Performance of GSM 900 Antenna in the Presence of People and Phantom, *IEEE International Conference on Antennas and Propagation*, Vol. 1, pp. 35-38, March 2003

[5] Sadeghzadeh, R.A., McEwan, N.J. (1994). Prediction of Head Proximity Effect on Antenna Impedance Using Spherical Waves Expansions, *Electronics Letters,* Vol.6, No.4, pp. 844-847, August 1994

[6] Firrao, E.L., Ennema, A.J., Nauta, B., (2004). Antenna Behaviour in the Presence of Human Body, *15th Annual Workshop on Circuits, Systems and Signal Processing*, pp. 487-490, November 2004

[7] Song, H., Bakkaloglu, B., Aberle, J.T., (2009). A CMOS Adaptive Antenna-Impedance Tuning IC Operating in the 850 MHz to 2 GHz band, *IEEE International Solid-State Circuits Conference*, pp. 384-386, February 2009

[8] De Mingo, J., Valdovinos, A., Crespo, A., Navarro, D., Garcia, P., (2004). A RF Electronically Controlled Impedance Tuning Network Design and its Appliaction to an Antenna Input Impedance Matching System, *IEEE Transactions on Microwave Theory and Techniques*, vol. 52, no. 2, pp. 489-497, February 2004

[9] Sjöblom, P., Sjöland, H., (2005). An Adaptive Impedance Tuning CMOS Circuit for ISM 2.4 GHz Band, *IEEE Transactions on Circuits and Systems I: Regular Papers*, vol. 52, no. 6, pp. 1115-1124, June 2005

[10] Van Bezooijen, A., De Jongh, M.A., Chanlo, C., Ruijs, L.C.H., Van Straten, F., Mahmoudi, R., Van Roermund, H.M., (2008). A GSM/EDGE/WCDMA Adaptive Series LC Matching Network Using RF-MEMS Switches, *IEEE Journal on Solid-State Circuits*, vol. 43, no. 10, pp. 2259-2268, October 2008

[11] Firrao, E.L., Annema, A.J., Nauta, B., (2008). An Automatic Antenna Tuning System Using Only RF-Signal Amplitudes, *IEEE Transactions on Circuits and Systems II: Express Briefs*, vol. 55, no. 9, pp. 833-837, September 2008

[12] Song, H., Oh, S.H., Aberle, J.T., Bakkaloglu, B., Chakrabarti, C., (2007). Automatic Antenna Tuning Unit for Software-Defined and Cognitive Radio, *IEEE International Symposium on Antennas and Propagation*, pp. 85-88, June 2007

[13] Van Bezooijen, A., De Jongh, M.A., Van Straten, F., Mahmoudi, R., Van Roermund, A.H.M., (2010). Adaptive Impedance-Matching Techniques for Controlling L Networks, *IEEE Transactions on Circuits and Systems I: Regular Papers*, vol. 57, no. 2, pp. 495-505, February 2010

[14] Fu, J., Mortazawi, A., (2008). Improving Power Amplifier Efficiency and Linearity Using a Dynamically Controlled Tunable Matching Network, *IEEE Transactions on Microwave Theory and Techniques*, vol. 56, no. 12, pp. 3239-3244, December 2008

[15] Neo, E.W.C., Lin, Y., Liu, X., De Vreede, L.C.N., Larson, L.E., Spirito, M., Pelk, M.J., Buisman, K., Akhnoekh, A., De Graauw, A., Nanver, L.K., (2006). Adaptive Multi-Band Multi-Mode Power Amplifier Using Integrated Varactor-Based Tunable Matching Networks, *IEEE Journal on Solid-State Circuits*, vol. 41, no. 9, pp. 2166-2176, September 2006

[16] Lakin, K.M., McCarron, K.T., Rose, R.E. (1995). Solid Mounted Resonators and Filters, *IEEE International Ultrasonics Symposium*, vol. 2, pp. 905-908, November 1995

[17] Aigner, R. et al. (2003). Bulk Acoustic Wave Filters: Performance Optimization and Volume Manufacturing, IEEE MTT-S, pp. 2001-2004, 2003

[18] Kim J., Rahmat-Samii, Y. (2004). Implanted antennas inside a human body simulations, designs and characterizations, *IEEE Transactions on Microwave Theory and Techniques*, vol. 52, no. 8, pp. 1934-1943, August 2004

[19] Soontornpipit, P., Furse, C.M., Chung, Y.C., (2004). Design of Implantable Microstrip Antenna for Communication with Medical Implants, *IEEE Transactions on Microwave Theory and Techniques*, vol. 52, no. 8, pp. 1944-1951, August 2004

[20] Soontornpipit, P., Furse, C.M., Chung, Y.C., (2004). Miniaturized Biocompatible Microstrip Antenna Using Genetic Algorithm, *IEEE Transactions on Antennas and Propagation*, vol. 53, no. 6, pp. 1939-1945, June 2005

[21] Lee, C.M., Yo, T.C., Luo, C.H., Tu, C.H., Juang, Y.Z., (2007). Compact Broadband Stacked Implantable Antenna for Biotelemetry with Medical Devices, *Electronic Letters*, vol. 43, no. 12, pp. 660-662, June 2007

[22] Bradley P.D. (2006). An Ultra Low Power High Performance Medical Implant Communication System (MICS) transceiver for Implantable Devices, *IEEE Biomedical Circuits and Systems Conference*, pp. 158-161, November 2006

[23] Evaluating Compliance with FCC Guidelines for Human Exposure to Radiofrequency Electromagnetic Fields, Office Eng. Tech., FCC, Washington DC, FCC OET Bull. 65, Supp. C

[24] CST Microwave Studio, Computer System Technology, GmbH, Darmstadt, Germany

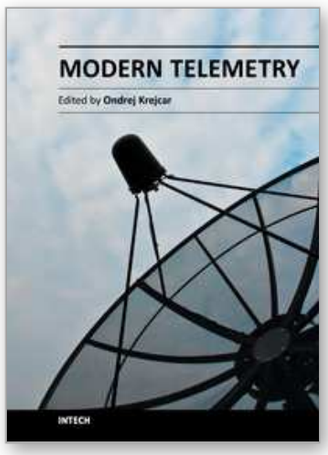
[25] Chan Wai Po, F., De Foucauld, E., Delavaud, C., Ciais, P., Kerhervé, E., (2008). A Vector Automatic Matching Network Designed for Wireless Medical Telemetry, *IEEE NEWCAS-TAISA joint Conference*, pp. 89-92, June 2008

[26] Yan, Y., Perreault, D.J. (2006). Analysis and Design of High Efficiency Matching Networks, *IEEE Transactions on Power Electronics*, vol. 21, no. 5, pp. 1484-1491, September 2006

[27] Chan Wai Po, F., de Foucauld, E., Morche, D., Vincent, P., Kerhervé, E. (2011). A Novel Method for Synthesizing an Automatic Matching Network and Its Control Unit, *IEEE Transactions on Circuits and Systems I: Regular paper*, vol. 58, Issue 11, November 2011

[28] Ludwig, R., Bogdanov, G., (2000). RF Circuit Design: Theory and Applications, 2nd edition Upper Saddle River, NJ: Prentice-Hall, 2000

[29] Chan Wai Po, F., de Foucauld, E., Vincent, P., Hameau, F., Morche, D., Delavaud, C., dal Molin, R., Pons, P., Pierquin, R., Kerhervé, E. (2009). A Fast and Accurate Automatic Matching Network Designed for Ultra Low Power Medical Applications, *IEEE International Symposium on Circuits and Systems*, pp. 673-676, May 2009



Modern Telemetry
Edited by Dr. Ondrej Krejcar

ISBN 978-953-307-415-3
Hard cover, 470 pages
Publisher InTech
Published online 05, October, 2011
Published in print edition October, 2011

Telemetry is based on knowledge of various disciplines like Electronics, Measurement, Control and Communication along with their combination. This fact leads to a need of studying and understanding of these principles before the usage of Telemetry on selected problem solving. Spending time is however many times returned in form of obtained data or knowledge which telemetry system can provide. Usage of telemetry can be found in many areas from military through biomedical to real medical applications. Modern way to create a wireless sensors remotely connected to central system with artificial intelligence provide many new, sometimes unusual ways to get a knowledge about remote objects behaviour. This book is intended to present some new up to date accesses to telemetry problems solving by use of new sensors conceptions, new wireless transfer or communication techniques, data collection or processing techniques as well as several real use case scenarios describing model examples. Most of book chapters deals with many real cases of telemetry issues which can be used as a cookbooks for your own telemetry related problems.

How to reference
In order to correctly reference this scholarly work, feel free to copy and paste the following:

Francis Chan Wai Po, Emeric de Foucauld, Jean-Baptiste David, Christophe Delavaud and Pascal Ciais (2011). An Efficient Adaptive Antenna-Impedance Tuning Unit Designed for Wireless Pacemaker Telemetry, Modern Telemetry, Dr. Ondrej Krejcar (Ed.), ISBN: 978-953-307-415-3, InTech, Available from: http://www.intechopen.com/books/modern-telemetry/an-efficient-adaptive-antenna-impedance-tuning-unit-designed-for-wireless-pacemaker-telemetry

INTECH
open science | open minds

InTech Europe
University Campus STeP Ri
Slavka Krautzeka 83/A
51000 Rijeka, Croatia
Phone: +385 (51) 770 447
Fax: +385 (51) 686 166
www.intechopen.com

InTech China
Unit 405, Office Block, Hotel Equatorial Shanghai
No.65, Yan An Road (West), Shanghai, 200040, China
中国上海市延安西路65号上海国际贵都大饭店办公楼405单元
Phone: +86-21-62489820
Fax: +86-21-62489821

© 2011 The Author(s). Licensee IntechOpen. This is an open access article distributed under the terms of the Creative Commons Attribution 3.0 License, which permits unrestricted use, distribution, and reproduction in any medium, provided the original work is properly cited.

IntechOpen

IntechOpen